Title

Noninvasive measurement of pressure gradient across a coronary stenosis using phase contrast (PC)-MRI: A feasibility study

Journal

Magnetic Resonance in Medicine, 77(2)

ISSN

0740-3194

Authors

Deng, Zixin
Fan, Zhaoyang
Lee, Sang-Eun
et al.

Publication Date

2017-02-01

DOI

10.1002/mrm.26579

Peer reviewed

HHS Public Access

Author manuscript

Magn Reson Med. Author manuscript; available in PMC 2017 August 15.

Published in final edited form as:

Magn Reson Med. 2017 February ; 77(2): 529–537. doi:10.1002/mrm.26579.

Noninvasive Measurement of Pressure Gradient Across a Coronary Stenosis Using Phase Contrast (PC)-MRI: A Feasibility Study

Zixin Deng[1,2], **Zhaoyang Fan**[1], **Sang-Eun Lee**[3], **Christopher Nguyen**[1], **Yibin Xie**[1], **Jianing Pang**[1], **Xiaoming Bi**[4], **Qi Yang**[1], **Byoung-Wook Choi**[5], **Jung-Sun Kim**[3], **Daniel Berman**[1], **Hyuk-Jae Chang**[3,*], and **Debiao Li**[1,2,6,*]

[1]Biomedical Imaging Research Institute, Department of Biomedical Sciences, Cedars-Sinai Medical Center, Los Angeles, California, USA

[2]Department of Bioengineering, University of California, Los Angeles, California, USA

[3]Division of Cardiology, Severance Cardiovascular Hospital, Seoul, South Korea

[4]Siemens Healthcare R&D, Los Angeles, California, USA

[5]Department of Radiology, Severance Hospital, Seoul, South Korea

[6]Department of Medicine, University of California, Los Angeles, California, USA

Abstract

Purpose—To investigate the feasibility of blood pressure difference measurement, ΔP, across the coronary artery using phase contrast (PC)-MRI for potential noninvasive assessment of the functional significance of coronary artery stenosis.

Methods—Three-directional velocities in the coronary arteries acquired using 2D-PC-MRI were used with the Navier-Stokes equations to derive ΔP. Repeat phantom studies were performed to assess the reproducibility of flow velocity and ΔP. ΔP derived using PC-MRI (ΔP_{MR}) and that obtained using pressure transducer (ΔP_{PT}) were compared. Reproducibility of coronary flow velocity was assessed in healthy controls (n = 11). Patients with suspected coronary artery disease (n = 6) were studied to evaluate the feasibility of ΔP_{MR} measurement across a coronary stenosis.

Results—*Phantom*: Good overall reproducibility of flow velocity and ΔP measurements and excellent correlation (ΔP_{MR} vs ΔP_{PT}) was observed: intraclass correlation (ICC) of 0.95(V_z), 0.72(V_x), 0.73(V_y), and 0.87(ΔP_{MR}) and R^2 =0.94, respectively. *Human*: Good reproducibility of coronary flow velocity was observed: ICC of 0.94/0.95(V_z), 0.76/0.74(V_x), and 0.80/0.77(V_y) at cardiac phase 1/2. Significant (p=0.025) increase in ΔP_{MR} was observed in patients (6.40 ± 4.43 mmHg) versus controls (0.70 ± 0.57 mmHg).

Conclusion—ΔP_{MR} in the coronary arteries is feasible. Upon further validation using the invasive measure, ΔP_{MR} has the potential for noninvasive assessment of coronary artery stenosis.

*Correspondence to: Debiao Li, Ph.D., Biomedical Imaging Research Institute, Cedars-Sinai Medical Center, 8700 Beverly Boulevard, PACT Suite 800, Los Angeles, CA 90048, USA. Debiao.Li@cshs.org; or Hyuk-Jae Chang, M.D., Ph.D., Division of Cardiology, Severance Hospital, Yonsei University College of Medicine, 50-1 Yonsei-ro, Seodaemun-gu, Seoul, South Korea, 120-752. hjchang@yuhs.ac.

Keywords

fractional flow reserve (FFR); magnetic resonance imaging (MRI); phase-contrast MRI (PC-MRI); relative pressure difference estimation; coronary artery disease (CAD); coronary pressure gradient

INTRODUCTION

Fractional flow reserve (FFR) is a measure of the functional significance of coronary stenosis in patients with coronary artery disease (CAD) (1,2). It can be obtained by the ratio of the blood pressure distal to a stenosis (P_d) and the aortic pressure (P_a) averaged over a few cardiac cycles, respectively, during invasive coronary angiography (ICA). The procedure is performed during maximal hyperemia to ensure a constant (near zero) intracoronary resistance (3). Similar intracoronary resistance could be achieved at rest if P_a and P_d are measured during middle to end diastole of the cardiac cycle, denoted as instantaneous wave-free ratio (iFR) (4). Studies have shown that an FFR of ≤0.80 and/or an iFR index of ≤0.89 is more accurate for identifying a functionally significant stenosis that may cause myocardial ischemia and thus require revascularization than the use of a visually estimated 70% diameter stenosis (DS) alone (1). In addition, a strong linear correlation ($r = 0.81$; $P < 0.001$) between FFR and iFR was observed, where an iFR index of ≤0.89 correctly classified 82.5% of the stenosis when compared against an FFR index of ≤0.80 (5). Although FFR is still the clinical gold standard for the functional assessment of a stenotic coronary lesion, iFR is gradually utilized in combination with FFR in clinical routine (6,7).

Both FFR and iFR are invasive procedures associated with potential complications, high costs, and extra time during the intra-arterial procedure. In addition, the rate of nonobstructive (<50% DS) and nonischemia inducing (FFR > 0.80) stenosis remains high during invasive catheterization, resulting in unnecessary procedures (8,9). A noninvasive pressure gradient measurement will be useful to serve as a gatekeeper to eliminate unnecessary invasive procedures. Recent noninvasive technique using coronary computed tomographic angiography (CCTA) in combination with computational fluid dynamics simulations to estimate the functional significance of coronary artery stenosis, denoted as FFR_{CT}, has shown promise (10). However, it requires the exposure to ionizing radiation and is prone to blooming artifacts caused by heavy calcification (11).

In this study, we evaluate a noninvasive pressure gradient measurement technique across the coronary artery using phase-contrast MRI (PC-MRI). MRI has the advantage of no ionizing radiation, allowing longitudinal monitoring of CAD patients. PC-MRI directly measures the blood flow velocity and has been used to derive the pressure difference (ΔP) in the cardiac chamber (12–15), aorta (16–19), carotid (20,21), iliac (21), renal (22), and intracranial (23,24) arteries using the Navier Stokes (NS) analysis. Highly significant correlations (R^2= 0.91 and $R^2 = 0.95$) between ΔP derived from PC-MRI and that measured using a pressure wire were observed in relatively small and semistationary vessels (carotid/iliac (21) and renal (22) arteries, respectively) with ~50% to 60% DS. However, it has not been used in the coronary artery because of the small size and mobility of the vessel.

The purpose of this study is to assess the feasibility of noninvasive ΔP measurement using PC-MRI in stenotic phantoms and healthy and diseased coronary arteries. Stenotic phantom experiments were first performed to evaluate the reproducibility of flow velocity and ΔP measurements using PC-MRI and NS analysis, respectively. ΔP measurements derived using PC-MRI (ΔP_{MR}) and that obtained using a pressure transducer (ΔP_{PT}) were compared. A pilot study was then performed in healthy controls and a small cohort of stable CAD patients to evaluate the feasibility of ΔP_{MR} measurement in the coronary arteries. A MR-iFR index, similar to FFR/iFR, was estimated based on ΔP_{MR} to observe the trend of this index in different coronary artery stenosis.

METHODS

Sequence Design

A 2D spoiled gradient recalled echo, PC-MRI, sequence with a conventional four-point velocity-encoding scheme (reference, x, y, z) was used for image acquisition on a 3.0 Tesla (T) MR system (Verio; Siemens Healthcare GmbH, Erlangen, Germany) (25). To minimize cardiac and respiratory motion effects, the acquisition window was limited to diastole and end-expiration using electrocardiogram (ECG) triggering and navigator gating, respectively, as shown in Figure 1. To ensure the total acquisition time per cardiac cycle is within the quiescent phase, a view sharing (VS) technique, where data were shared between different cardiac phases, was implemented (26). The three-directional velocity vector field (V_x, V_y, and V_z) from all cross-sectional coronary artery slices and two cardiac phases was used as input parameters for pressure gradient estimation using NS equations (14,16).

Pressure Difference Estimation

To obtain the pressure difference (ΔP) across a region of interest (ROI), the NS equations were used to investigate the relationship between velocity and pressure. The NS equations, as shown below in the Cartesian form, express the conservation of momentum of a nonturbulent, incompressible Newtonian fluid (14,16,19,22) (Eq. [1]):

$$-\frac{\partial P}{\partial x_i}=\rho\frac{\partial v_i}{\partial t}+\rho\left[v_1\frac{\partial v_i}{\partial x_1}+v_2\frac{\partial v_i}{\partial x_2}+v_3\frac{\partial v_i}{\partial x_3}\right]-\mu\left[\frac{\partial^2 v_i}{\partial x_1^2}+\frac{\partial^2 v_i}{\partial x_2^2}+\frac{\partial^2 v_i}{\partial x_3^2}\right]-F_i,\ \ i=x,\ y,\ z \quad [1]$$

where P is pressure, ρ is fluid density, μ is fluid dynamic viscosity, and F includes the body force terms. On the right-hand side of the equation, the terms from left to right represent the transient inertia (local acceleration), three convective inertia components, viscous friction terms, and the gravitational force. The x_is are the x-, y-, and z-axes in the image frame, and the v_is are the corresponding velocity components. To calculate the temporal $[\partial v_i/\partial t]$ and spatial $[\partial v_i/\partial x_{1;2;3}]$ first-order velocity derivatives, a forward difference approximation at the pixel with maximum coronary velocity identified in each PCMRI cross-sectional slice was used. Using the maximum velocity could avoid any partial volume errors caused by the limited spatial resolution at the stenotic regions of the phantom or the coronary artery. Because of the narrowness of the phantom tubing and the coronary artery, it is spatially limited to accurately calculate the spatial second-order velocity derivatives $[\partial^2 v_i/\partial x^2_{1,2,3}]$;

therefore, to prevent any unwanted error, the viscosity terms were ignored assuming inviscid flow. In addition, because the phantom and human subjects were horizontally positioned in the scanner during MR acquisition with minimal influence from gravity, the body force terms (F_i), which includes gravity, is also neglected. The simplified form of the NS equation (Euler's equation, neglecting gravity) is used for all calculations as shown below (Eq. [2]):

$$-\frac{\partial P}{\partial x_i}=\rho\left[\frac{\partial v_i}{\partial t}+v_1\frac{\partial v_i}{\partial x_1}+v_2\frac{\partial v_i}{\partial x_2}+v_3\frac{\partial v_i}{\partial x_3}\right],\ i=x,y,z \quad [2]$$

Two methods were explored to obtain the pressure gradients. Velocity gradients from all three directions were first analyzed. Given that the in-plane velocities are small and may have minimal contribution to the overall pressure gradient, velocity gradient from through-plane direction only was also analyzed to explore this phenomenon.

From the derived pressure gradients [$\partial P/\partial x_i$] where $x_i = x, y, z$ in the image frame, pressure difference [ΔP] was then calculated using integration along a path (12,14), as represented in the equation below (Eq. [3]):

$$\Delta P=\sum_i\left[\left(\frac{\partial P}{\partial x}\right)_i\Delta x_i+\left(\frac{\partial P}{\partial y}\right)_i\Delta y_i+\left(\frac{\partial P}{\partial z}\right)_i\Delta z_i\right],\ i=slice\ number \quad [3]$$

where Δx_i, Δy_i, and Δz_i are the vector length of each linear segment along a predefined path determined by connecting the maximum velocity points of consecutive cross-sectional slices, assuming integration is not path dependent (12,14). The total pressure difference, ΔP, is then calculated as the sum of all segments shown in Equation [3].

Experiments

The feasibility of the technique was demonstrated in stenotic phantom, healthy controls, and stable CAD patients. Scans were performed on a MAGNETOM Verio and Trio 3.0T MRI system (Siemens Healthcare) equipped with a 32-channel (Invivo, Gainesville, FL, USA) and body array matrix coil, respectively. Validation of the flow velocity and ΔP measurements was first performed in stenotic phantoms, followed by reproducibility study of the velocity measurements in healthy controls (n = 11). CCTA and/or invasive catheterization (ICA and/or FFR) was performed in patients (n = 6) and compared to the proposed technique. All human studies where approved by the institutional review board and written consent was obtained before imaging.

Validation of Velocity and ΔP Measurements in Stenotic Phantoms—A schematic of the phantom design is shown in figure 2a. Twelve stenotic phantoms (reference inner diameter [ID] = 4.8 mm) at 0% to 60% DS were individually connected to a flow pump (Masterflex; Cole-Parmer, Vernon Hills, IL, USA) that pumped gadolinium (Gd)-doped water (density of ~1000 kg/m^3) at a constant volume velocity of 250 mL/min while 2D PC-MRI images were acquired. Imaging parameters were: field of view (FOV) = (215 × 215 mm)^2; flip angle (FA) = 15°; echo time (TE) = 3.86 to 4.51 ms; repetition time (TR) =

67.12 to 73.92 ms; in-plane spatial resolution =(0.50–0.58 × 0.50–0.58 mm)^2; slice thickness = 3.2 mm; V_{enc} = z (40–260 cm/s) and x, y (40–80 cm/s), depending on %DS. Repeat scans were performed in seven of the twelve phantoms to assess reproducibility. Immediately following the PC-MRI scans, pressure was measured using a pressure transducer (Invivo), as shown in Figure 2a, before and after the maximum narrowing. Examples of PC-MRI images are shown in Figure 2b.

Reproducibility of Coronary Velocity in Healthy Controls—Eleven healthy controls (2 females; average age, 47.3 ± 14.6 years; group A) were recruited and two repeat PC-MRI scans were performed to assess reproducibility. The intervals between the repeat acquisitions were approximately 5 minutes apart to avoid any physiological changes that could potentially alter the velocity measurements. Imaging protocol was: 1) targeted free-breathing contrast enhanced (0.20 mmol/kg of Gd-BOPTA [MultiHance, Bracco Imaging SpA, Milano, Italy] at 0.30 mL/s) 3D fast low angle shot (3D-FLASH) coronary magnetic resonance angiography (cMRA) for coronary localization; 2) cross-sectional image locations across the coronary segments of interest were obtained using 3D multiplanar reconstruction and used for PC-MRI scans; and 3) free-breathing 2D coronary PC-MRI with fat suppression to avoid chemical shift effects and increase vessel contrast (27,28). Approximately four to nine contiguous PC-MRI imaging slices were consecutively collected across the coronary segment of interest. Imaging parameters were: FOV = (215 × 215 mm)^2 with 10% to 50% oversampling in the phase encode, depending on subject size; FA = 15° ; V_{enc} = 35 to 45 cm/s in all three orthogonal directions; cardiac phase = 2 (~70 ms/phase); in-plane spatial resolution =(0.5–0.6 × 0.5–0.6 mm)^2; slice thickness = 3.2 mm; and time of acquisition = 3 to 5 min/image slice.

Validation of Coronary ΔP Measurements in Patients—Seven patients (3 females; average age, 68 ± 7.7 years) with new-onset or recurrent stable chest pain were enrolled. Patient inclusion criteria were: patients with 1) known or suspected stable CAD and 2) at least one suspected left coronary artery stenosis at the proximal to middle region detected by CCTA and/or ICA. Patient exclusion criteria were: patients with 1) acute coronary syndrome (acute myocardial infarction or unstable angina); 2) previous coronary revascularization (coronary bypass surgery and/or stenting); 3) contradiction to Gd contrast; and 4) non-MRI compatible implants and/or claustrophobia. One patient was excluded because of poor PC-MRI image quality (limited spatial resolution and minor motion artifact).

Imaging studies and analysis were performed in all 6 patients. Five of the 6 patients (group B) have nonobstructive coronary stenosis (3 patients with ICA of <50% DS and 2 without ICA have CCTA of <70% DS) and no invasive FFR. One of the 6 patients has an obstructive (diffused, 50% DS) and functionally significant (FFR = 0.56) coronary stenosis (group C) at the left anterior descending (LAD) coronary artery. CCTA, ICA, and FFR (Volcano Inc., Rancho Cordova, CA, USA) measurements of all patients were obtained from their routine clinical records.

Similar imaging protocol and parameters as healthy controls were used. The difference between the two consists of: 1) 0.20 mmol/kg of Gd-DOTA (Dotarem; Guerbet Group, Villepinte, France) at 0.20 mL/s; 2) V_{enc} =35 to 65 cm/s in three orthogonal directions,

depending on %DS shown from CCTA and/or cMRA, and/or obtained from a V_{enc} scout; and 3) imaging slices were collected across the stenotic lesion of interest (location matched to invasive catheterization). PC-MRI reproducibility was not tested, because scan time was limited.

Data Analysis

All PC-MRI images were directly reconstructed on the MR scanner. PC-MRI image corrections and NS analysis were performed using a customized MATLAB program (The Mathworks, Inc., Natick, MA, USA). The resultant image data set includes: one flow compensated image and three magnitude image sets and three phase image sets in x, y, and z directions, respectively, per cardiac phase. A total of two cardiac phases were collected, resulting in a total of 14 images per cross-sectional slice. Image-based eddy current corrections were performed in all PC-MRI images before NS analysis (29,30).

To calculate the pressure difference (ΔP_{MR}) from PC-MRI, ROIs were first drawn on the magnitude images and mapped onto its corresponding velocity images to obtain the maximum velocities for NS analysis. Density of fluid and blood was 1000 and 1060 kg/m^3 for *in vitro* and *in vivo* ΔP_{MR} estimations, respectively. ΔP_{MR} derived using velocity gradients from all three directions (ΔP_{MR}) and from through-plane direction only ($\Delta P_{MR\text{-}Vz}$) were explored. Note that velocities used for $\Delta P_{MR\text{-}Vz}$ calculations were not acquired separately in this study. Because the proposed technique is a measure of the relative pressure difference ($\Delta P = P_a - P_d$), when comparing with invasive pressure measurements, a P_a of 74.2 mm Hg (31) was used when calculating the MR index: MR-iFR = $P_d/P_a = (P_a - \Delta P)/P_a$. It is important to note that the proposed technique was acquired at rest and during diastole only, thus similar to an iFR technique.

To calculate the pressure difference (ΔP_{PT}) from the pressure transducer, differences of the recorded pressure values at the two measurement locations (before and after the maximum narrowing) were obtained. The %DS of each phantom model was calculated from 3D-FLASH, anatomical, images using the maximum and minimum diameters measured in OsiriX (Pixmeo, Bernex, Switzerland).

In phantom studies, reproducibility of the peak velocity and ΔP_{MR} measurements were assessed and the correlation between ΔP_{MR} and ΔP_{PT} and $\Delta P_{MR\text{-}Vz}$ and ΔP_{PT} were evaluated. In human studies, reproducibility of the peak flow velocities was assessed in healthy controls and ΔP_{MR} for both healthy controls and patients were then statistically compared. In addition, MR-iFR index was calculated in all patients. Example cases are described to show the feasibility of the proposed technique.

Statistical Analysis

In all tests, statistical significance was defined at $P < 0.05$. Intraclass correlation coefficient (ICC) was calculated using SPSS software (v.16.0; IBM SPSS Statistics, Armonk, NY, USA) to test the statistical significant of similarity, and standard Bland-Altman plots were obtained using GraphPad Prism software (GraphPad Software Inc., La Jolla, CA, USA) to analyze the agreement between repeat PC-MRI scans. Unpaired two-tailed Student *t* test was used to determine any statistically significant differences, and linear regression analysis was

used with the least-squares method to assess correlation between data sets (Microsoft Excel, Redmond, WA, USA). All numerical data are presented as mean ± standard deviation.

RESULTS

Validation of Velocity and ΔP Measurements in Stenotic Phantoms

A total of 10 to 20 cross-sectional slices were acquired for each stenotic phantom. Table 1 represents the reproducibility of peak velocity and ΔP_{MR} measurements in its %DS groups (1. 35–45%; 2. 45–55%; 3. 55–60%;) and all together. Overall, excellent ICC was observed in the V_z encoding direction and slightly lower in V_x and V_y. When comparing between %DS groups, peak velocity and ΔP_{MR} measurements showed higher ICCs in the lower %DS groups and relatively lower ICCs as %DS increased. Little bias was observed from the Bland-Altman plots of the peak velocities (Fig. 3a) and ΔP_{MR} measurements (Fig. 3b). An exponential relationship was observed between ΔP_{MR} and %DS (Fig. 3c). In addition, excellent correlations (R^2=0.938 and R^2=0.904) were observed between ΔP_{MR} and ΔP_{PT} (Fig. 3d) and $\Delta P_{MR\text{-}Vz}$ and ΔP_{PT}, respectively.

Reproducibility of Coronary Velocity in Healthy Controls

A total of four to nine cross-sectional slices across a coronary segment (healthy controls) or stenotic lesion (patients) were acquired for each subject. In healthy controls (group A), excellent ICCs were observed in the through-plane peak velocities (V_z; 0.94 and 0.95) for cardiac phase 1 and 2 and slightly lower in V_x (0.76 and 0.74) and V_y (0.80 and 0.77), respectively. Reproducibility of the ΔP_{MR} measurement in healthy controls was not assessed because the values were near zero. A significant (P = 0.025) increase in ΔP_{MR} was noted in the patient group (6.40 ± 4.43 mm Hg) versus healthy controls (0.70 ± 0.57 mm Hg; Fig. 4). MR-iFR index of patients and healthy controls were 0.91 ± 0.06 and 0.99 ± 0.01, respectively.

Validation of Coronary ΔP Measurement in Patients

Five of the 6 patients (group B) had nonobstructive coronary stenosis found by CCTA and/or ICA. Relatively small pressure drop or higher MR-iFR index (ΔP_{MR} = 4.73 ± 1.93 mm Hg or MR-iFR = 0.94 ± 0.03) was observed using the proposed noninvasive MRI method, respectively. One of the 6 patients (group C) has an obstructive (diffused, 50% DS) and functionally significant (FFR = 0.56) coronary stenosis at proximal LAD (pLAD) by ICA and invasive FFR, respectively. Relatively high pressure drop or lower MR-iFR index (ΔP_{MR}≈15 mm Hg or MR-iFR = 0.80) was observed using the proposed noninvasive MRI method. Example images from groups B and C are shown in Figures 5 and 6, respectively.

ΔP_{MR} measurement derived using through-plane velocity gradients only was also explored in both patient groups. A $\Delta P_{MR\text{-}Vz}$ or MR-iFR$_{Vz}$ index of 3.85 ± 1.89 mm Hg or 0.95 ± 0.03 and ~7 mm Hg or 0.91 was observed in group B and group C, respectively.

DISCUSSION

In this work, we have demonstrated the feasibility of a noninvasive blood pressure gradient measurement technique in the coronary arteries using PC-MRI. The proposed method has the advantage of being a noninvasive technique with no ionizing radiation. Phantom and human studies have demonstrated the feasibility of velocity and pressure gradient measurements in small-sized vessel using PC-MRI and NS analysis, respectively. Phantom studies showed a high correlation between ΔP_{MR} and ΔP_{PT} with overall good reproducibility of the peak flow velocity and ΔP_{MR} measurements. Human studies demonstrated the feasibility of coronary flow velocity and ΔP_{MR} measurements in both healthy and diseased coronary arteries. In addition, the MR-iFR results across the three groups studied (A: controls, B: patients with nonobstructive coronary stenosis, and C: patient with obstructive and functionally significant stenosis) have shown consistent trends with that of invasive FFR in literature.

Specifically, in vivo studies showed close to zero ΔP_{MR} or MR-iFR index close to 1 in healthy controls, slight pressure drop (higher ΔP_{MR}, 4.73 mm Hg) or lower MR-iFR index (~0.94) in patients with nonobstructive stenosis and relatively high ΔP (~15 mm Hg) or low MR-iFR index (~0.80) in patients with obstructive and functionally significant stenosis. This trend is consistent with the general tendency of invasive FFR, where healthy coronaries have no significant decline of pressure, FFR close to 1 (close to zero ΔP), and, as the %DS and functional significance of a coronary lesion increases, a lower FFR value was observed (higher ΔP) (3). The lesion is then considered an ischemia-inducible stenosis if FFR is ≤0.80 (high ΔP) (32).

A recent noninvasive technique, FFR_{CT}, has shown promise in deferring patients from unnecessary invasive procedures. However, the technique exposes patients to ionizing radiation. In addition, a small subset of CCTA images suffer from poor image quality for FFR_{CT} analysis partially attributed to excessive calcium blooming (33), which could potentially be mitigated through the use of MRI. In one patient case, where obstructive coronary artery stenosis (heavy calcification, > 70% DS) was initially reported by CCTA, the proposed technique subsequently showed $\Delta P_{MR} \approx 3$ mm Hg or MR-iFR ≈ 0.96, suggestive of a low likelihood of a significant stenosis. The discrepancy was then later confirmed by ICA, showing a nonobstructive lesion (<30% DS), confirming the PC-MRI results. A major advantage of MRI is the ability to perform a comprehensive examination of CAD in the same setting. The proposed technique can be potentially combined with MR myocardial perfusion imaging for the assessment of reduced blood flow to myocardium and that caused by a specific coronary stenosis, which could be useful in making treatment decisions. In addition, MRI is a purely noninvasive technique that uses no ionizing radiation or invasive catheterization. This proposed technique could serve as an additional complementary noninvasive functional test that could potentially provide lesion-specific diagnosis before invasive catheterization. This may potentially allow for a more-effective risk stratification and better differentiation of patients who would most likely benefit from invasive catheterization, therefore, reduce any unnecessary invasive procedures (8,34).

In this study, ΔP_{MR} derived using velocity gradients from all three directions (ΔP_{MR}) and from through-plane direction only ($\Delta P_{MR\text{-}Vz}$) were both explored. In phantoms, good correlation was observed in both methods when comparing to ΔP_{PT}. In patients, in-plane velocity may have a higher contribution at higher stenotic levels given that an approximately 50% underestimation was observed in group C compared to B. In vitro and in vivo studies demonstrated the potential of using through-plane velocities only, thus allowing for shorter scan times. Although underestimation was observed in vivo, a new cut-off value could potentially be established to help determine the functionally severity of a stenosis.

The performance of the proposed method can be further improved. Because of the small size of coronary arteries, especially at stenotic regions, partial volume effects, residual cardiac and respiratory motion, and higher orders of fluid motion (ie, turbulence) could affect the accuracy of the PC-MRI velocity measurements. Spatial resolution of PC-MRI has been discussed in literature as one of the main factors affecting the accuracy of ΔP_{MR} measurements (35). Casas et al has shown that a ΔP underestimation of up to a 5.8% average difference could be found when approximately three voxels remain in the x and y directions and up to 10.9% if approximately two voxels remain (36). The current study focused in patients with <70% DS because patients with 70% to 99% DS shown in CCTA are considered to have severe obstructive CAD where ICA is recommended for risk assessment (37,38). If we consider an average of 50% DS in a 3-mm-diameter coronary segment, approximately three residual pixels remain if a 0.5×0.5 mm^2 in-plane resolution is used. However, because ΔP_{MR} was shown to increase exponentially with increase in %DS (Fig. 3c), in a clinical setting, the estimated ΔP_{MR} for a functionally significant stenotic lesion may still remain above the prescribed cut-off value (threshold) despite the error. Nevertheless, to better understand the accuracy and robustness of the technique, future technical development in higher-spatial-resolution PC-MRI and larger-scale patient studies are required. Advanced techniques, such as radial acquisition and motion correction, could make the measurement more motion robust (39,40). Higher spatial resolution may result in lower signal-to-noise ratio, where 3D coronary PC-MRI could be implemented. With the improvement in spatial resolution, techniques such as iterative refinement could be implemented to obtain a pressure difference map (19) across the coronary artery and viscosity terms that were ignored in this study could be incorporated. In addition, in the current study, the integration path was defined by connecting the maximum velocity pixels in consecutive cross-sections to exploit high velocity-to-noise ratio. However, integration along a streamline (path parallel to the velocity field at a single instant in time) or pathline (path of particles as they move through space over time) and its effect on the accuracy of the MR-iFR measurements need to be explored.

It is important to note that ΔP_{MR} measurements were acquired at one single time point (Δt in diastole) only, mimicking an iFR technique. To ultimately obtain an invasive FFR index, higher temporal resolution measurements from the entire cardiac cycle is needed with adenosine administration. Furthermore, age, sex, and other potential confounders were not controlled in this study and are needed in the future studies. More patients with invasive FFR are underway to determine the MR-iFR cut-off value to differentiate between functionally significant and non-significant stenosis.

CONCLUSION

Our preliminary studies demonstrated the feasibility of a noninvasive pressure gradient measurement in the coronary arteries using PC-MRI. Upon further validation, this approach has the potential to serve as a gatekeeper to prevent unnecessary invasive catheterization procedures in patients with CAD.

Acknowledgments

Grant sponsor: Leading Foreign Research Institute Recruitment Program; Grant sponsor: National Research Foundation of Korea (NRF); Grant sponsor: Ministry of Science, ICT & Future Planning (MSIP); Grant number: 2012027176.

Grant sponsors: This research was supported by Leading Foreign Research Institute Recruitment Program through the National Research Foundation of Korea (NRF) funded by the Ministry of Science, ICT & Future Planning (MSIP); Grant number: 2012027176.

References

1. Tonino PA, De Bruyne B, Pijls NH, et al. Fractional flow reserve versus angiography for guiding percutaneous coronary intervention. N Engl J Med. 2009; 360:213–224. [PubMed: 19144937]
2. Berry C, van't Veer M, Witt N, et al. VERIFY (VERification of Instantaneous Wave-Free Ratio and Fractional Flow Reserve for the Assessment of Coronary Artery Stenosis Severity in EverydaY Practice). J Am Coll Cardiol. 2013; 61:1421–1427. [PubMed: 23395076]
3. Pijls NH, Van Gelder B, Van der Voort P, Peels K, Bracke FA, Bonnier HJ, Gamal el MI. Fractional flow reserve. A useful index to evaluate the influence of an epicardial coronary stenosis on myocardial blood flow. Circulation. 1995; 92:3183–3193. [PubMed: 7586302]
4. Sen S, Escaned J, Malik IS, et al. Development and validation of a new adenosine-independent index of stenosis severity from coronary wave-intensity analysis: results of the ADVISE (ADenosine Vasodilator Independent Stenosis Evaluation) study. J Am Coll Cardiol. 2012; 59:1392–1402. [PubMed: 22154731]
5. Escaned J, Echavarría-Pinto M, Garcia-Garcia HM, et al. Prospective assessment of the diagnostic accuracy of instantaneous wave-free ratio to assess coronary stenosis relevance: Results of ADVISE II International, Multicenter Study (ADenosine Vasodilator Independent Stenosis Evaluation II). JACC Cardiovasc Interv. 2015; 8:824–833. [PubMed: 25999106]
6. Härle T, Bojara W, Meyer S, Elsäasser A. Comparison of instantaneous wave-free ratio (iFR) and fractional flow reserve (FFR) - First real world experience. Int J Cardiol. 2015; 199:1–7. [PubMed: 26179896]
7. Fede A, Zivelonghi C, Benfari G, et al. iFR-FFR comparison in daily practice: a single-center, prospective, online assessment. J Cardiovasc Med (Hagerstown). 2015; 16:625–631. [PubMed: 26090913]
8. Patel MR, Dai D, Hernandez AF, Douglas PS, Messenger J, Garratt KN, Maddox TM, Peterson ED, Roe MT. Prevalence and predictors of non-obstructive coronaryartery disease identified with coronary angiography incontemporary clinical practice. Am Heart J. 2014; 167:846–852.e2. [PubMed: 24890534]
9. Tonino PA, Fearon WF, De Bruyne B, Oldroyd KG, Leesar MA, Ver Lee PN, MacCarthy PA, Van't Veer M, Pijls NH. Angiographic versus functional severity of coronary artery stenoses in the FAME study. J Am Coll Cardiol. 2010; 55:2816–2821. [PubMed: 20579537]
10. Nørgaard BL, Leipsic J, Gaur S, et al. Diagnostic performance of noninvasive fractional flow reserve derived from coronary computed tomography angiography in suspected coronary artery disease: the NXT trial (Analysis of Coronary Blood Flow Using CT Angiography: Next Steps). J Am Coll Cardiol. 2014; 63:1145–1155. [PubMed: 24486266]

11. Park MJ, Jung JI, Choi YS, Ann SH, Youn HJ, Jeon GN, Choi HC. Coronary CT angiography in patients with high calcium score: evaluation of plaque characteristics and diagnostic accuracy. Int J Cardiovasc Imaging. 2011; 27:43–51. [PubMed: 22048849]
12. Ebbers T, Wigstrom L, Bolger AF, Engvall J, Karlsson M. Estimation of relative cardiovascular pressures using time-resolved three-dimensional phase contrast MRI. Magn Reson Med. 2001; 45:872–879. [PubMed: 11323814]
13. Ebbers T, Wigström L, Bolger AF, Wranne B, Karlsson M. Noninvasive measurement of time-varying three-dimensional relative pressure fields within the human heart. J Biomech Eng. 2002; 124:288–293. [PubMed: 12071263]
14. Thompson RB, McVeigh ER. Fast measurement of intracardiac pressure differences with 2D breath-hold phase-contrast MRI. Magn Reson Med. 2003; 49:1056–1066. [PubMed: 12768584]
15. Nagao T, Yoshida K, Okada K, Miyazaki S, Ueguchi T, Murase K. Development of a noninvasive method to measure intravascular and intracardiac pressure differences using magnetic resonance imaging. Magn Reson Med Sci. 2008; 7:113–122. [PubMed: 18827454]
16. Yang GZ, Kilner PJ, Wood NB, Underwood SR, Firmin DN. Computation of flow pressure fields from magnetic resonance velocity mapping. Magn Reson Med. 1996; 36:520–526. [PubMed: 8892202]
17. Tasu JP, Mousseaux E, Delouche A, Oddou C, Jolivet O, Bittoun J. Estimation of pressure gradients in pulsatile flow from magnetic resonance acceleration measurements. Magn Reson Med. 2000; 44:66–72. [PubMed: 10893523]
18. Tyszka JM, Laidlaw DH, Asa JW, Silverman JM. Three-dimensional, time-resolved (4D) relative pressure mapping using magnetic resonance imaging. J Magn Reson Imaging. 2000; 12:321–329. [PubMed: 10931596]
19. Bock J, Frydrychowicz A, Lorenz R, Hirtler D, Barker AJ, Johnson KM, Arnold R, Burkhardt H, Hennig J, Markl M. In vivo noninvasive 4D pressure difference mapping in the human aorta: phantom comparison and application in healthy volunteers and patients. Magn Reson Med. 2011; 66:1079–1088. [PubMed: 21437978]
20. Turk AS, Johnson KM, Lum D, Niemann D, Aagaard-Kienitz B, Consigny D, Grinde J, Turski P, Haughton V, Mistretta C. Physiologic and anatomic assessment of a canine carotid artery stenosis model utilizing phase contrast with vastly undersampled isotropic projection imaging. AJNR Am J Neuroradiol. 2007; 28:111–115. [PubMed: 17213435]
21. Lum DP, Johnson KM, Paul RK, Turk AS, Consigny DW, Grinde JR, Mistretta CA, Grist TM. Transstenotic pressure gradients: measurement in swine—retrospectively ECG-gated 3D phase-contrast MR angiography versus endovascular pressure-sensing guidewires. Radiology. 2007; 245:751–760. [PubMed: 18024452]
22. Bley TA, Johnson KM, François CJ, Reeder SB, Schiebler ML, R Landgraf B, Consigny D, Grist TM, Wieben O. Noninvasive assessment of transstenotic pressure gradients in porcine renal artery stenoses by using vastly undersampled phase-contrast MR angiography. Radiology. 2011; 261:266–273. [PubMed: 21813739]
23. Miyati T, Mase M, Kasai H, Hara M, Yamada K, Shibamoto Y, Soellinger M, Baltes C, Luechinger R. Noninvasive MRI assessment of intracranial compliance in idiopathic normal pressure hydrocephalus. J Magn Reson Imaging. 2007; 26:274–278. [PubMed: 17610284]
24. Moftakhar R, Aagaard-Kienitz B, Johnson K, Turski PA, Turk AS, Niemann DB, Consigny D, Grinde J, Wieben O, Mistretta CA. Noninvasive measurement of intra-aneurysmal pressure and flow pattern using phase contrast with vastly undersampled isotropic projection imaging. AJNR Am J Neuroradiol. 2007; 28:1710–1714. [PubMed: 17885239]
25. Pelc NJ, Bernstein MA, Shimakawa A, Glover GH. Encoding strategies for three-direction phase-contrast MR imaging of flow. J Magn Reson Imaging. 1991; 1:405–413. [PubMed: 1790362]
26. Deng Z, Xie G, He Y, et al. Pressure gradient measurement in the coronary artery using view-sharing (VS) 4D PC-MRI: towards noninvaisve quantification of fractional flow reserve. International Society of Magnetic Resonance Imaging in Medicine (ISMRM Annual Meeting). 2014:1.
27. Middione MJ, Ennis DB. Chemical shift-induced phase errors in phase-contrast MRI. Magn Reson Med. 2013; 69:391–401. [PubMed: 22488490]

28. Keegan J, Raphael CE, Parker K, et al. Validation of high temporal resolution spiral phase velocity mapping of temporal patterns of left and right coronary artery blood flow against Doppler guidewire. J Cardiovasc Magn Reson. 2015; 17:85. [PubMed: 26428627]
29. Lorenz R, Bock J, Snyder J, Korvink JG, Jung BA, Markl M. Influence of eddy current, Maxwell and gradient field corrections on 3D flow visualization of 3D CINE PC-MRI data. Magn Reson Med. 2014; 72:33–40. [PubMed: 24006013]
30. Bock, J., Kreher, BW., Hennig, J., Markl, M. Optimized pre-processing of time-resolved 2D and 3D phase contrast MRI data. Proceedings of the 15th Annual Meeting of ISMRM; Berlin, Germany. 2007. p. 3138
31. Williams B, Lacy PS, Yan P, Hwee CN, Liang C, Ting CM. Development and validation of a novel method to derive central aortic systolic pressure from the radial pressure waveform using an N-point moving average method. J Am Coll Cardiol. 2011; 57:951–961. [PubMed: 21329842]
32. Pijls NHJ, Fearon WF, Tonino PAL, et al. Fractional flow reserve versus angiography for guiding percutaneous coronary intervention in patients with multivessel coronary artery disease: 2-year follow-up of the FAME (Fractional Flow Reserve Versus Angiography for Multivessel Evaluation) study. J Am Coll Cardiol. 2010; 56:177–184. [PubMed: 20537493]
33. Douglas PS, Pontone G, Hlatky MA, et al. Clinical outcomes of fractional flow reserve by computed tomographic angiography-guided diagnostic strategies vs. usual care in patients with suspected coronary artery disease: the prospective longitudinal trial of FFR CT: outcome and resource impacts study. Eur Heart J. 2015; 36:3359–3367. [PubMed: 26330417]
34. Patel MR, Peterson ED, Dai D, Brennan JM, Redberg RF, Anderson HV, Brindis RG, Douglas PS. Low diagnostic yield of elective coronary angiography. N Engl J Med. 2010; 362:886–895. [PubMed: 20220183]
35. Nasiraei-Moghaddam A, Behrens G, Fatouraee N, Agarwal R, Choi ET, Amini AA. Factors affecting the accuracy of pressure measurements in vascular stenoses from phase-contrast MRI. Magn Reson Med. 2004; 52:300–309. [PubMed: 15282812]
36. Casas B, Lantz J, Dyverfeldt P, Ebbers T. 4D flow MRI-based pressure loss estimation in stenotic flows: evaluation using numerical simulations. Magn Reson Med. 2015; 75:1808–1821. [PubMed: 26016805]
37. Leipsic J, Yang TH, Thompson A, Koo BK, Mancini GB, Taylor C, Budoff MJ, Park HB, Berman DS, Min JK. CT angiography (CTA) and diagnostic performance of noninvasive fractional flow reserve: results from the Determination of Fractional Flow Reserve by Anatomic CTA (DeFACTO) study. AJR Am J Roentgenol. 2014; 202:989–994. [PubMed: 24758651]
38. Fihn SD, Gardin JM, Abrams J, et al. 2012 ACCF/AHA/ACP/AATS/PCNA/SCAI/STS Guideline for the Diagnosis and Management of Patients With Stable Ischemic Heart Disease: A Report of the American College of Cardiology Foundation/American Heart Association Task Force on Practice Guidelines, and the American College of Physicians, American Association for Thoracic Surgery, Preventive Cardiovascular Nurses Association, Society for Cardiovascular Angiography and Interventions, and Society of Thoracic Surgeons. Circulation. 2012; 126:e354–e471. [PubMed: 23166211]
39. Kecskemeti S, Johnson K, Wu Y, Mistretta C, Turski P, Wieben O. High resolution three-dimensional cine phase contrast MRI of small intracranial aneurysms using a stack of stars k-space trajectory. J Magn Reson Imaging. 2011; 35:518–527. [PubMed: 22095652]
40. Pang J, Bhat H, Sharif B, Fan Z, Thomson LE, LaBounty T, Friedman JD, Min J, Berman DS, Li D. Whole-heart coronary MRA with 100% respiratory gating efficiency: Self-navigated three-dimensional retrospective image-based motion correction (TRIM). Magn Reson Med. 2013; 71:67–74. [PubMed: 23401157]

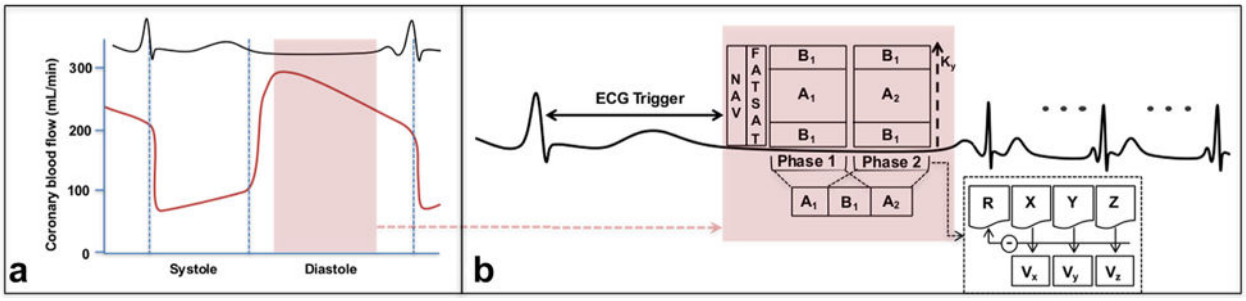

FIG. 1.

(**a**) Coronary flow timing diagram. Graph from Arthur Guyton et al, Textbook of Medical Physiology, (Elsevier Inc.; Copyright 2006). Phase-contrast (PC)-MRI acquisition was obtained during diastole. (**b**) Sequence design. ECG-triggered, navigator-gated, 2D PC-MRI with three-directional velocity encoding (V_x, V_y, and V_z). VS was implemented to restrict the acquisition within the quiescent phase, two cardiac phases (phase 1 and phase 2) were obtained. NAV=navigator; FATSAT=fat suppression prepulse; B=peripheral k-space (B_1); A=center k-space (A_1 and A_2).

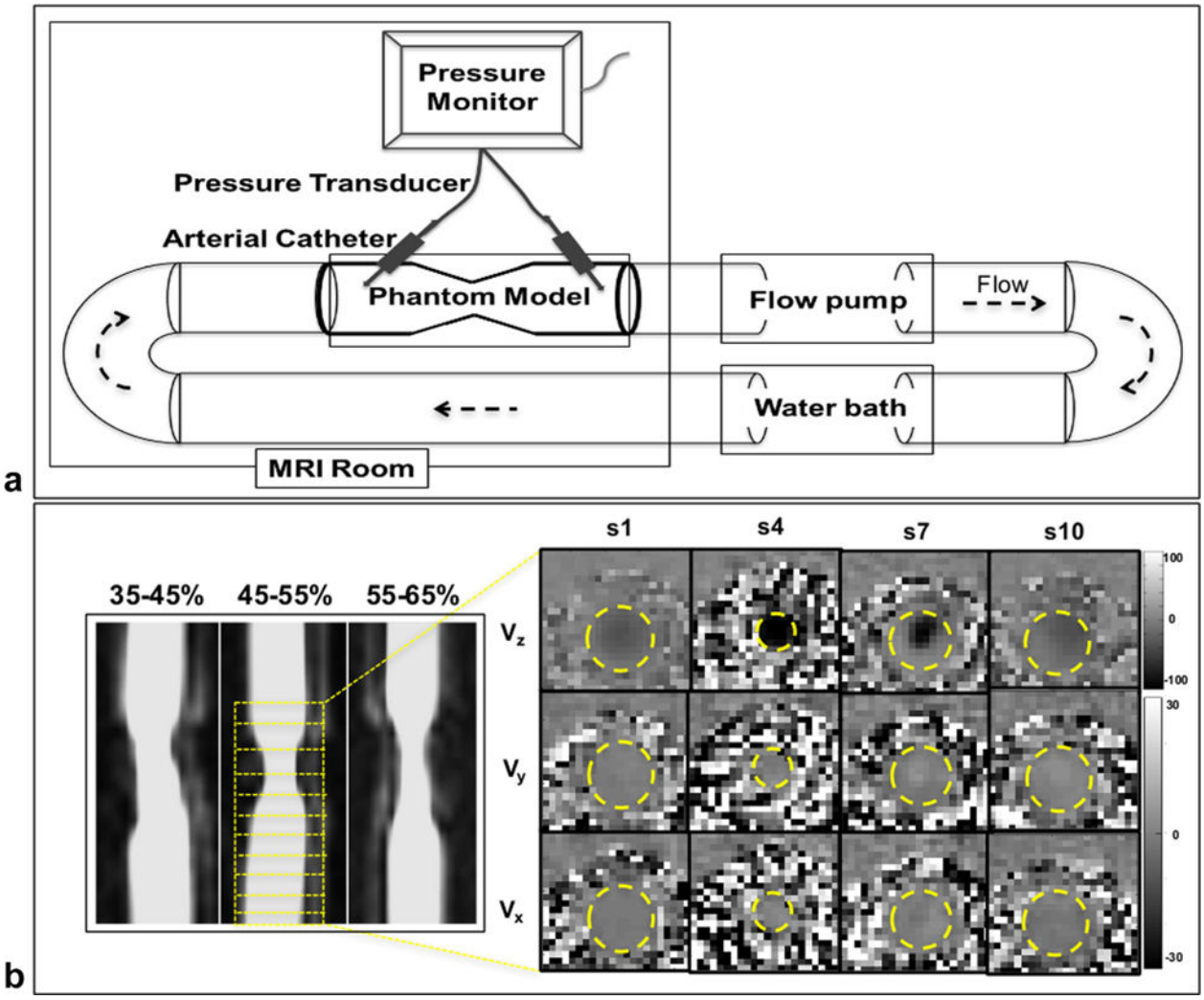

FIG. 2.

(**a**) Schematic of the stenotic phantom model design. (**b**) Stenotic phantom model examples at different range of % diameter stenosis and 2D PC-MRI images in the through-plane (V_z) and in-plane (V_y, V_x) directions (velocity maps, cm/s) for 45% to 55% diameter stenosis phantom model. S = slice number.

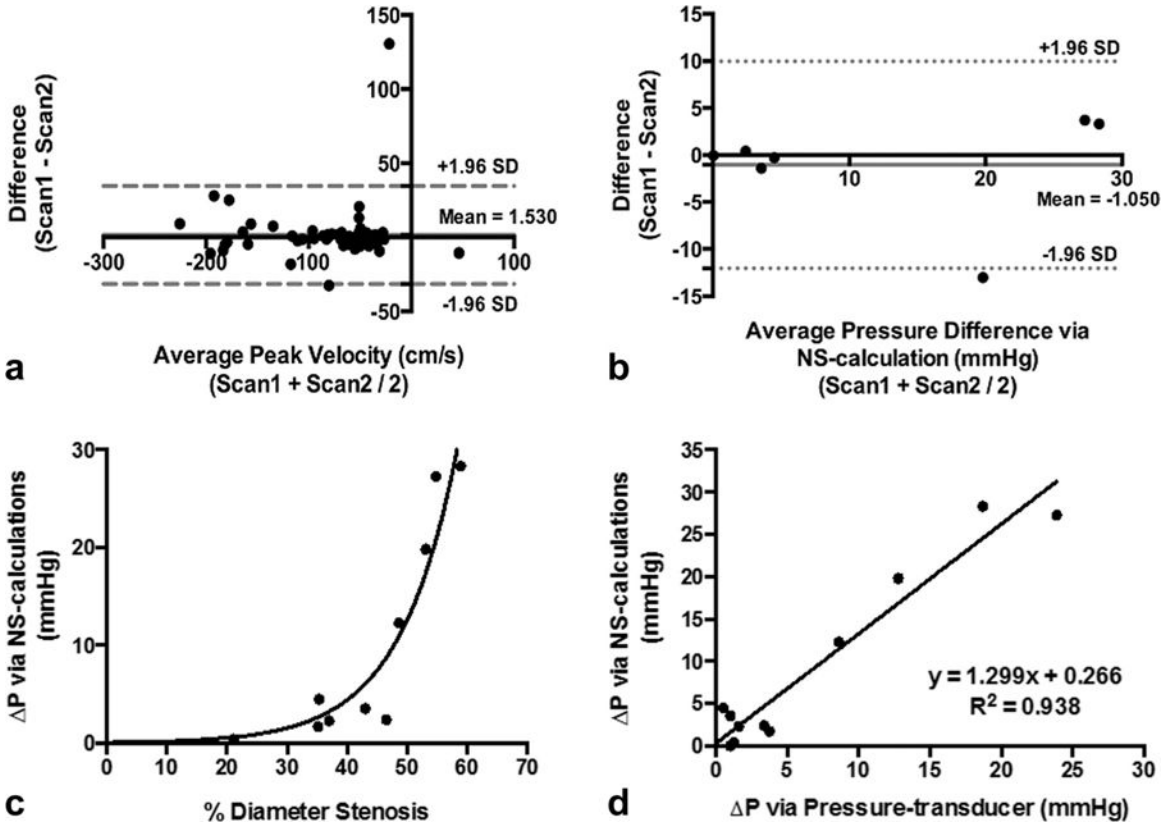

FIG. 3.

Bland-Altman plots of (**a**) peak velocities (bias of 1.530; 95% confidence interval [CI], −31.49 to 34.55) at all cross-sectional slice from repeat PC-MRI scans and (**b**) ΔP_{MR} of the stenotic phantoms (bias of −1.050; 95% CI, −12.03 to 9.934). Mean (bias) and 95% CI limits are displayed. (**c**) ΔP_{MR} measurement versus % diameter stenosis. An exponential increase in ΔP_{MR} was observed as % diameter stenosis increases. (**d**) Comparison between ΔP calculated by NS equations (ΔP_{MR}) and ΔP measured using pressure transducer (ΔP_{PT}). Excellent correlation ($R^2 = 0.94$) was observed between the two techniques.

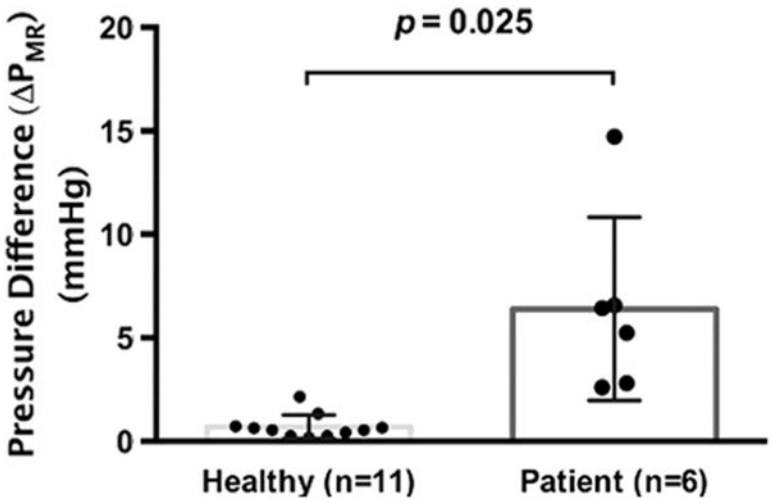

FIG. 4.

ΔP_{MR} of healthy control and patient groups. A significant ($P = 0.025$) increase in ΔP_{MR} was noted in the patient group (6.40 ± 4.43 mm Hg) compared against the healthy controls (0.70 ± 0.57 mm Hg).

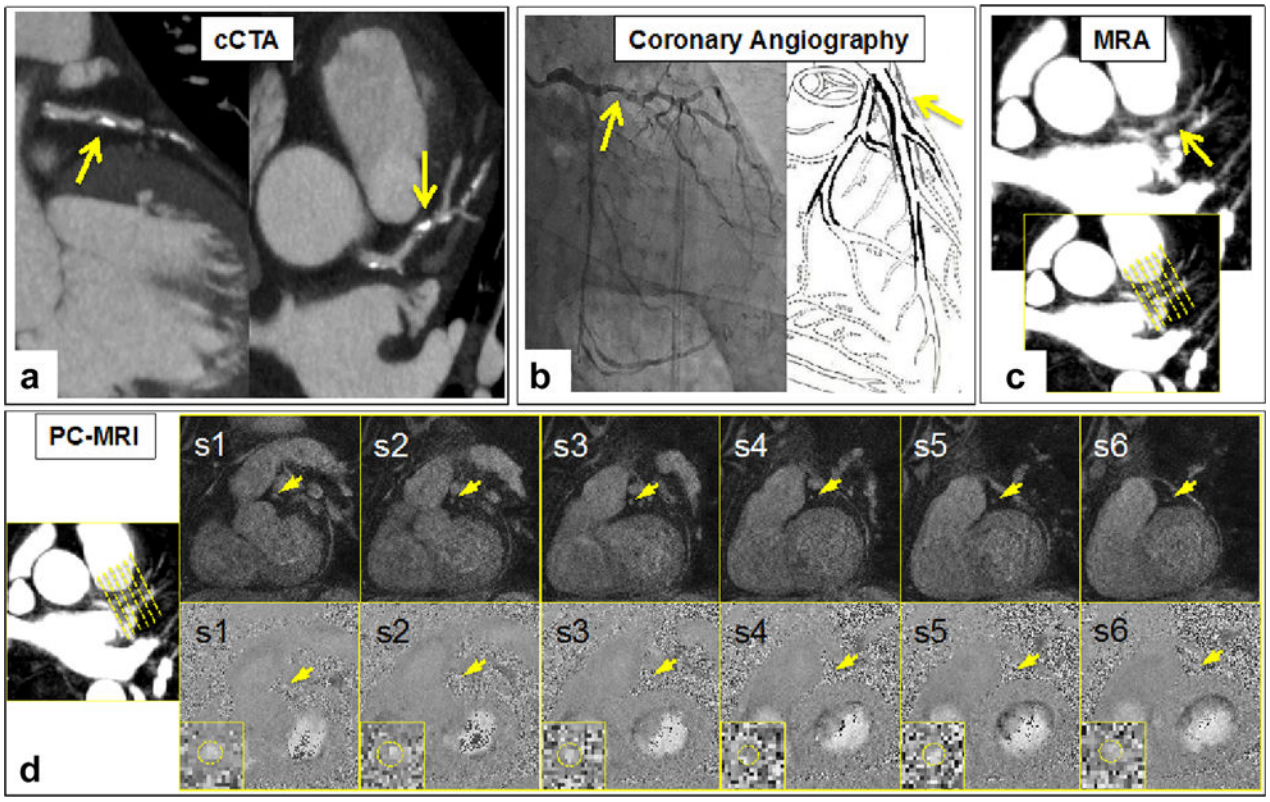

FIG. 5.

(**a**) Coronary CTA of the pLAD artery reported as >70% calcified stenosis. (**b**) Invasive coronary angiography reported as minimum lumen narrowing (<30% stenosis), nonsignificant lesion. (**c**) MRA of the pLAD. (**d**) PC-MRI (eight imaging slices) across the stenotic lesion at the pLAD artery. Top row: flow compensated images; bottom row: PC-MRI (velocity map) images represented in the Vz-direction. ΔP_{MR} was approximately 3 mm Hg or MR-iFR ≈0.96. S = slice number.

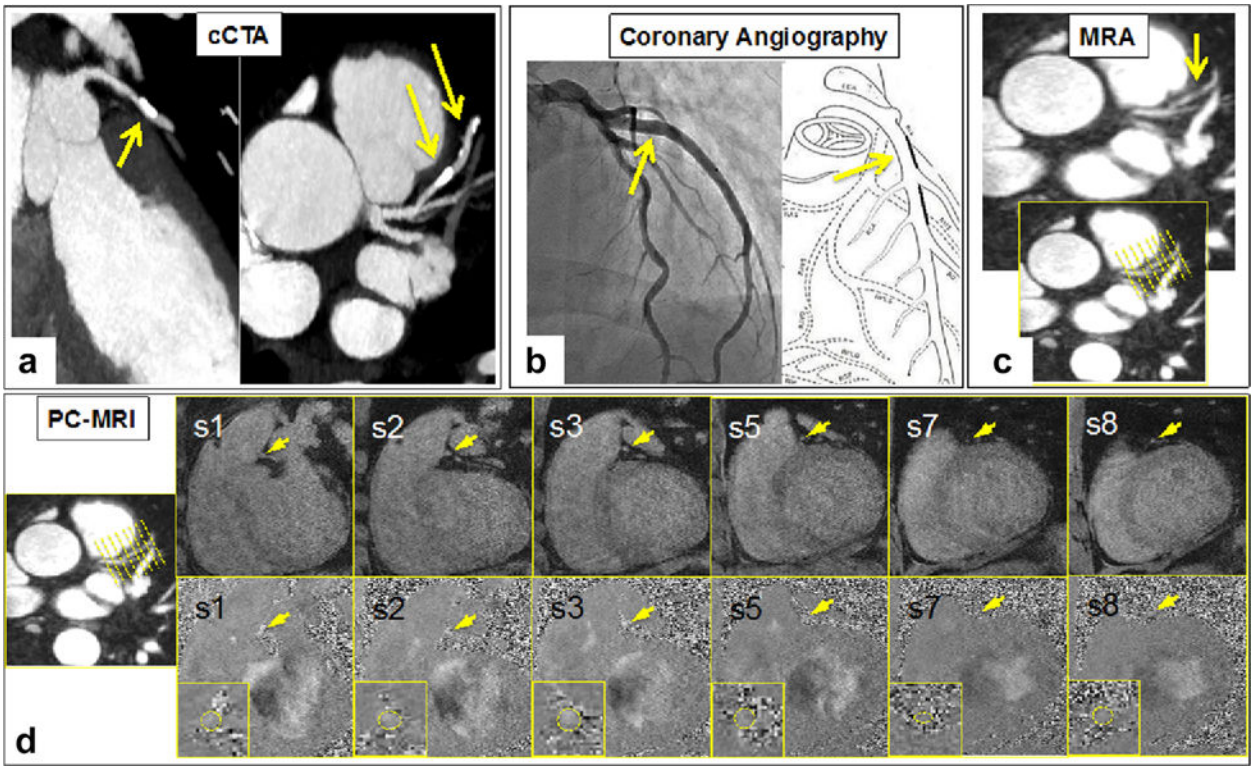

FIG. 6.

(**a**) Coronary CTA of the pLAD artery. (**b**) Invasive coronary angiography showing diffused irregular lesion, with 50% lumen narrowing and FFR of 0.56 (functionally significant lesion). (**c**) MRA of the pLAD. (**d**) PC-MRI (six imaging slices) across the stenotic lesion at the pLAD. Top row: flow compensated images; bottom row: PC-MRI (velocity map) images represented in the V_z-direction; ΔP_{MR} was approximately 15 mm Hg or MR-iFR ≈0.80. S = slice number.

Table 1

ICC of Peak Velocities and ΔP_{MR} Measurement of the Stenotic Phantoms

	Peak Velocity (ICC)			
Stenotic Phantoms (% Diameter Stenosis)	**V_z**	**V_x**	**V_y**	**ΔP_{MR} (ICC)**
35 to 45 (n = 1)	0.998	0.839	0.868	0.976
45 to 55 (n = 2)	0.999 ± 0.00	0.857 ± 0.05	0.853 ± 0.12	0.964 ± 0.01
55 to 60 (n = 3)	0.950 ± 0.07	0.558 ± 0.10	0.640 ± 0.24	0.859 ± 0.12
All (n = 7)	0.948	0.724	0.731	0.867